Delayed heating calculations using the MCNP-ORIGEN Activation Automation tool

Roberto E. Fairhurst-Agosta,[*,a] and Tomasz Kozlowski[a]

[a] *Department of Nuclear, Plasma, and Radiological Engineering*
University of Illinois Urbana-Champaign, Urbana, IL 61801

[*]Email: ref3@illinois.edu

Number of pages: 29
Number of tables: 1
Number of figures: 8

Abstract

An accurate assessment of the deposited energy across a reactor geometry allows a better determination of the heat removal requirements and ensure effective cooling after shutdown. This work discusses several methods in detail that target the heat deposition in specific reactor regions, leading to a choice of a prevalent method for the calculation workflow. This article introduces a delayed heating calculation workflow based on the formal 3-step process. The workflow relies on the MCNP-ORIGEN Activation Automation tool for performing the first two steps of the process, while the third step is conducted via MCNP photon transport simulations. This article showcases two applications to demonstrate the workflow and simulation outputs. These include an Advanced Test Reactor experiment and the RA-6 reactor structures.

Keywords — Delayed Heating, MCNP, ORIGEN, ATR, RA-6

I. INTRODUCTION

In an operating reactor, an equilibrium exists between the generation and removal of heat. After reactor shutdown, radioactive decay continues to release energy, which is deposited across the reactor and causes the delayed heating. The estimation of delayed heating in experiments and in the reactor structures is paramount in the safety analyses of research reactors, and its accurate determination generates a reliable heat source term for thermal-hydraulics calculations. This in turn allows the determination of heat removal requirements and evaluation of temperature levels in the components of interest [1, 2, 3].

Additionally, detailed calculations help in the optimization process of the irradiation target designs [4]. Overall, these calculations determine whether delayed heating presents a hazard for the components of interest, which could lead to the release of radioactive contaminants into the reactor coolant. An important application example is in spent nuclear fuel where delayed heating calculations are crucial for the design of nuclear facilities, including spent fuel storage pools, spent fuel transportation systems, reprocessing plants, and final storage sites.

In research reactors, the safety analysis process places a strong focus on the reactor core. Numerous studies have targeted diverse accidents in research reactors, such as the loss-of-coolant accident (LOCA) and the loss-of-flow accident (LOFA). Kazeminejad et al. [5] investigated the peak fuel and cladding temperatures of a 10-MW IAEA research reactor after a LOFA with flow inversion. Meanwhile, Hainoun et al. [6] introduced a benchmark exercise for thermal-hydraulic codes studying a LOFA in the IEA-R1 research reactor, and Abdelmaksoud et al. [7] examined the passive heat removal by natural convection and radiation of a typical research reactor after a LOCA. These studies rely on different versions of the ANSI/ANS standard [8] for estimating the decay heat after reactor shutdown, which assumes that the energy released after shutdown is deposited locally in the region of interest, i.e., the reactor core. This assumption is echoed by several other software packages such as Serpent [9, 10] and ORIGEN [11], which estimate the decay heat by assuming the local deposition of heat, and several studies relied on the same assumption. Lee et al. [12] used ORIGEN-2 to compare the decay heat in a high-temperature gas-cooled reactor (HTGR) core containing transuranic and uranium fuel. Ilas et al. [13] calculated the decay heat in the High Flux Isotope Reactor (HFIR) irradiated fuel using ORIGEN-2.2, and Hawkes et al. [14] evaluated with ORIGEN-2.2 the thermal behavior of AGR-2, which is an Advanced Test Reactor

(ATR) fueled experiment for TRISO particles.

However, an accurate assessment of the deposited energy across the reactor geometry is required to better determine the heat removal requirements and ensure an effective cool down. Moreover, the regulatory authorities and the industry are interested in more precise calculations for uncertainty quantification (UQ) and economic reasons. Therefore, instead of assuming the local deposition of heat, this work focused on detailed methods targeting the specific reactor regions such as reactor experiments or reactor structures.

The objective of this article is to introduce a delayed heating calculation workflow based on the MCNP-ORIGEN Activation Automation (MOAA) tool [15, 1, 16, 17], present the motivation for the choice of the method, and showcase its capabilities by presenting two specific applications. The Irradiation Experiment Neutronics Analysis group at the Idaho National Laboratory (INL) developed MOAA to streamline the calculation of the experiment source terms for the ATR and the Transient Reactor Test Facility (TREAT). The calculated source terms have multiple applications, which include radiation shielding, inventory and shipping purposes, demonstration of compliance with the safety limits, modeling of radioactive material dispersion, comparison to post-irradiation examination (PIE) results for validation, and experiment design and optimization, among others.

Although MOAA was originally developed to analyze the irradiation of experiments at ATR, it has grown to become a more general tool through further development. At a higher level, MOAA is a tool that calculates radionuclide mass, activity, and heat in the regions of interest in a nuclear reactor. More specifically, MOAA is a python package that couples MCNP [18] and ORIGEN by writing MCNP tally cards, reading MCNP tallies, creating SCALE input files, executing SCALE, and standardizing the results post-processing. Streamlining this procedure helps to reduce processing times and avoid potential human errors. Further details on the motivation behind MOAA's development can be found in [15].

The rest of this article is organized as follows. Section II describes previous work using different methods to calculate delayed heating and further motivates the progress presented here. Section III details the main aspects of the calculation workflow. Section IV presents and discusses the results of delayed heating calculations in the ATR and the Argentine research reactor RA-6. Finally, Section V summarizes the contributions of this work and the calculation workflow to the nuclear engineering field.

II. BACKGROUND

The main contributions to the nuclear heating in an operating reactor can be summarized as follows [19]:

- Prompt neutron heating: deposition of the recoil energy of nuclei after a neutron collision and energy deposition of resulting charged particles from neutron interactions - e.g., heating caused by protons released in (n, p) interactions.
- Delayed neutron heating: energy deposition of resulting charged particles created with a delay after a neutron interaction - e.g., heating caused by alpha particles resulting from activation and fission product decay.
- Prompt gamma heating: energy deposition of resulting charged particles of photo-atomic and photo-nuclear interactions. Prompt photons are emitted right away after a neutron interaction. This includes prompt gamma radiation from the rapid de-excitation of the fission fragments and capture gammas.
- Delayed gamma heating: energy deposition mechanism same as prompt photons. Delayed photons are the result of activation and fission product decays.

After reactor shutdown, the prompt emissions no longer contribute to the heating, and we are left with only the delayed neutron and delayed gamma contributions. These contributions can be further classified by the location in which the emitted particles deposit their energy. The delayed neutron heating is caused by charged particles that deposit their energy locally due to their short range. The delayed gamma heating is caused by photons that deposit their energy globally and must be transported [4]. The following formula calculates the nuclear heating after reactor shutdown

$$H_{\mathrm{T}} = H_{\mathrm{ch}} + H_{\gamma,\mathrm{Tr}} \tag{1}$$

where H_{T} is the total heat deposited in the region of interest, H_{ch} is the energy deposited by charged particles in the region of interest, $H_{\gamma,\mathrm{Tr}}$ is the energy deposited in the region of interest resulting from photon transport.

A common method for the calculation of the delayed gamma contribution is the so-called Rigorous 2-Step (R2S) process [20]. Because the R2S process consists of three steps, this work refers to it as the *formal 3-step process*. This method consists of the following three steps:

- First, a neutron transport calculation determines the neutron flux spatial and energy distribution during reactor operation.
- Second, an activation calculation estimates the energy distribution and emission probability of the photon decays after reactor shutdown.
- Third, a photon-transport calculation evaluates the delayed gamma heating.

Earlier versions of this method accounted for the delayed photons through a fixed-source calculation based on pre-defined gamma emission probabilities. For example, Ambrosek et al. [21] used this method to calculate the delayed gamma heating component in two ATR experiment positions. Lee et al. [22] utilized pre-computed gamma emission probabilities from fission-product decay to calculate the gamma-radiation dose of several pressurized water reactor (PWR) spent fuel elements.

For the formal 3-step process, Mozin [23] utilized MCNP [18] and CINDER [24] to investigate the delayed gamma spectra sensitivity to the actinide content of spent LWR fuel. Lemaire et al. [19] utilized TRIPOLI-4 [25] and the point-depletion tool PEPIN-2 [26] to study the delayed photon contribution to the nuclear heating in the Jules Horowitz Reactor. Noh et al. [27] coupled MCNP and ORIGEN to study the delayed gamma heating by radiation originating in the activated structures of the High flux Advanced Neutron Application ReactOr (HANARO), a 30-MW research reactor of the Korea Atomic Energy Research Institute (KAERI).

Peterson-Droogh and Howard [4] summarized in a paper the modeling techniques for the calculation of the heating rates and the activity of iridium-192 targets in the HFIR at the Oak Ridge National Laboratory (ORNL). Their delayed heating calculation was separated into two methods. The first method was the PIKMT method, better detailed later in this article, for obtaining the delayed gamma contribution from fission product decay. The second method calculated the delayed gamma contribution from activation product decay using a coupling of MCNP and ORIGEN.

The dose rate evaluation of fusion reactor components is also another common application of the formal 3-step process. Chen et al. [20] calculated the shutdown dose rate of the ITER

mid-plane maintenance port coupling MCNP and the FISPACT inventory code [28]. Several other studies using this method include [29, 30].

Valenza et al. [31] introduced another method widely used for shutdown dose rate calculations in fusion reactors. The method replaces the prompt gamma spectrum with a decay gamma spectrum, and it is better known as the Direct 1-step (D1S) method. The method requires modifying the nuclear data library so that the delayed gamma radiation replaces the prompt gamma radiation. For example, the delayed gamma rays from Co-60 replace the prompt gamma rays that accompany the Co-59 (n, γ) reaction. Additionally, the method relies on an activation/depletion solver to account for the build-up and the decay of the considered radionuclides. Other fusion reactor studies [32, 33] used this same method. This method was also used to calculate the delayed gamma contribution in the HANARO core [27]. However, this method is most reliable if the generated radionuclides have short half-lives [27].

The *PIKMT* method has also become predominant in the past few years for delayed gamma heating calculations. It was first introduced by Brown et al. [34] and relies on the assumption that the prompt and delayed gamma spectra are similar. The method uses one neutron-photon coupled simulation using the MCNP PIKMT card to evaluate the energy deposited by prompt gamma radiation originating at fuel fission events, and then it scales it to the delayed gamma component. Ilas et al. [35] used the PIKMT method for calculating the heating rates in the HFIR's reflector during a highly-enriched uranium (HEU) to low-enriched uranium (LEU) conversion study. Davidson et al. [36] calculated the delayed gamma heating in different reactor regions using the PIKMT method for another HEU-to-LEU conversion study in HFIR. Jurbandam [37] calculated the spatial heat distribution in the SAFARI-1 nuclear reactor, relying on the PIKMT method to account for the delayed gamma contributions.

The overall performance of the PIKMT method has proven good. One of its main advantages over the formal 3-step process is that it requires only one coupled neutron/photon-transport simulation for obtaining the delayed gamma contribution. However, it only accounts for the gamma radiation emitted from fission product decay. In general, when the component of interest is in a close location to the fuel, the photons from fission product decay become the major contributor to the nuclear heating [19]. In other cases, the photons from activation product decay may have higher contributions. For those cases, only the formal 3-step process is applicable. Additionally,

the formal 3-step process obtains the charged particle contribution as a value-added of the calculation, which is a contribution that is neglected by the PIKMT method. Furthermore, the PIKMT method allows for obtaining the delayed gamma contribution during reactor operation or immediately after shutdown. Given that this work is concerned with the time evolution of the delayed heating, the only applicable method is the formal 3-step process.

III. METHODOLOGY

The first two steps in the formal 3-step process are accomplished by coupling a transport and a depletion solver, and there are several software packages available with these capabilities [38, 39, 40, 41]. Depletion solvers ignore the geometry of the system which signals the need for a transport solver. The transport solver generates geometry- and material-dependent parameters that the depletion solver relies on. The depletion solver then calculates the material compositions and returns this information to the transport solver, and a cyclical transfer of information occurs. The delayed heating calculation workflow presented here relies on MOAA for performing the first two steps of the process.

III.A. MOAA

MOAA performs material irradiation and decay calculations which can be configured to include a single or multiple irradiation steps. While a single-step calculation uses constant power irradiation, multi-step calculations handle several core configurations and piecewise constant power irradiation (i.e., different power levels at each time step). Such a capability allows for the modeling of evolution in material density, temperature, and geometry, as well as the control rod movement during the irradiation cycle. Additionally, the calculations can be configured to utilize the conventional predictor-corrector scheme, which is a two-step process that combines explicit and implicit calculations to achieve better convergence.

Figure 1 displays MOAA's main calculation workflow. The user input file (UIF) defines a list of irradiation cases, a list of decay times, and a list of MCNP cells defining the regions of interest. The irradiation case geometry and material definition are specified by the MCNP input file(s).

MCNP is a general-purpose, continuous-energy, generalized-geometry, Monte Carlo radiation-transport tool that can track neutrons, photons, electrons, and other particles. The main advantage

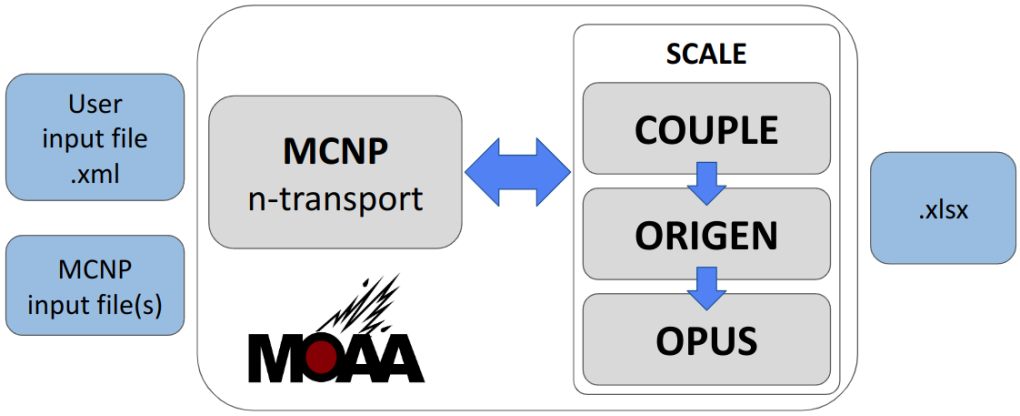

Fig. 1. Graphical representation of MOAA's workflow.

of the Monte Carlo method is its capability to model geometry and interaction physics without significant approximations. MOAA relies on MCNP for obtaining the geometry- and material-dependent parameters of the user-defined system - i.e., fluxes and one-group cross-sections - during the irradiation steps.

To accommodate the MOAA calculations, the MCNP input files must undergo a few minimal modifications. First, the independent depletion of cells sharing the same material composition requires an independent material definition in the input files.

Second, while MOAA can handle the depletion of cells defined as repeated structures, it cannot handle the depletion when the same cell is present in different nested structures. For example, if cell 100 is nested in cells 300 and 900 (100<300<900), and cell 100 is also nested in cells 400 and 900 (100<400<900), MOAA can handle only one of the two nested structures in one given simulation. To handle both nested structures, cell 400 would have to be redefined as 300 if the geometry definition allows, and MOAA will be able to handle both occurrences simultaneously.

Third, the volume of some depleted cells has to be calculated and specified within the MCNP input file. For cells defined as repeated structures, the user must specify the volume of the whole material in those cells that is present in the geometry.

ORIGEN is a general-purpose point depletion and decay tool to calculate isotopic concentrations, radiation source terms, and decay heat. ORIGEN is integrated into the SCALE code system, which is a modeling and simulation suite for nuclear safety analysis and design. MOAA uses the calculated parameters from the MCNP output files to define the SCALE input files. Besides

ORIGEN, MOAA also uses the COUPLE and OPUS modules from SCALE. ORIGEN requires a single space and spectrum-weighted cross-section library that MOAA generates using COUPLE. Meanwhile, OPUS provides the ability to extract specific data from the ORIGEN output libraries, perform unit conversions, and generate data for post-calculation analysis.

III.B. Delayed heating

The delayed heating calculation can be separated into two parts. The first part calculates the deposition of energy from charged particles H_{ch}. This part includes only the charged particles originating in the geometry of the component of interest. The second part calculates the deposition of energy from photons $H_{\gamma,\mathrm{Tr}}$. Because photons deposit their energy globally, photon transport is required, and this includes the photons originating from across the reactor.

Equation 1 along with the following equations describe the delayed heating

$$H_{\mathrm{ch}}[\mathrm{W}] = H_{\mathrm{T,L}} - H_{\gamma,\mathrm{L}} \tag{2}$$

$$H_{\gamma,\mathrm{Tr}}[\mathrm{W}] = 1.6022 \times 10^{-13}\mathrm{J}\cdot\mathrm{MeV}^{-1} \times {}^{*}F8[\mathrm{MeV}] \times \sum_i S_i \tag{3}$$

$$S_i[\gamma\cdot\mathrm{s}^{-1}] = \int_E \varphi_i^{\gamma}(E)dE \tag{4}$$

$$s_i[-] = S_i / \sum_j S_j \tag{5}$$

where H_{T} is the total heat deposited in the region of interest, H_{ch} is the energy deposited in the region of interest by charged particles, $H_{\gamma,\mathrm{Tr}}$ is the energy deposited in the region of interest resulting from the photon transport, $H_{\mathrm{T,L}}$ is the total decay heat, $H_{\gamma,\mathrm{L}}$ is the total gamma heating, ${}^{*}F8$ is the energy deposition calculated by an *F8 tally, S_i is the total photon emission rate from the region i, $\varphi_i^{\gamma}(E)$ the photon source energy distribution from region i, and s_i is the source cell emission probability.

Overall, the calculation scheme follows the formal 3-step process, in which MOAA conducts the first two steps, and multiple MCNP photon-transport simulations carry out the third step, calculating the delayed gamma heating. As shown in Figure 2, the nuclear heating calculation relies primarily on MOAA. MOAA calculates $H_{\mathrm{T,L}}$ and $H_{\gamma,\mathrm{L}}$ in the component of interest assuming those to be locally deposited.

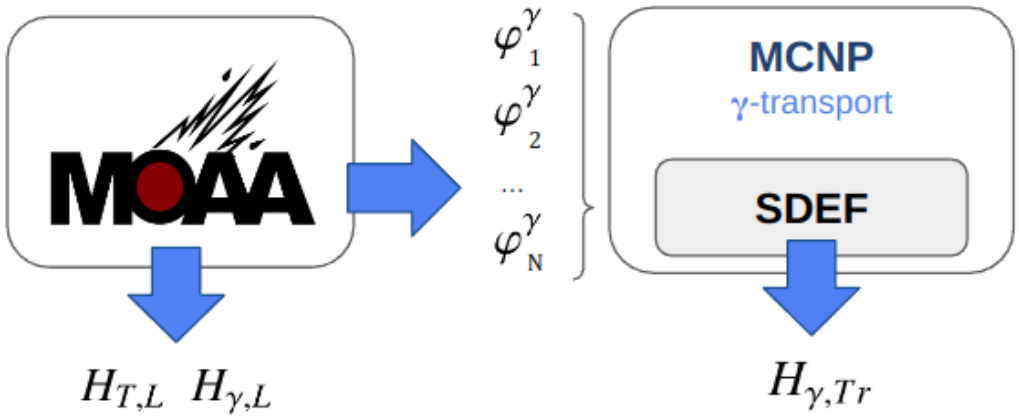

Fig. 2. Delayed heating calculation scheme relying on MOAA.

MOAA calculates $\varphi_i^{\gamma}(E)$ for all the cells defined by the user as contributors to the delayed heating. The MCNP photon-transport simulations require the definition of a fixed source for these cells. The source energy distribution is specified with $\varphi_i^{\gamma}(E)$.

The photon-transport calculation can be performed with multiple simulations, wherein one simulation obtains the heat contribution for one source cell, or with one simulation, wherein the simulation obtains the heat contribution for all the source cells simultaneously. While the former allows the determination of individual contributions from the different cells, the latter is computationally less expensive. Nonetheless, the latter requires the definition of the cell emission probabilities s_i using equation 5.

The source spatial distribution is assumed uniform in each source cell. For uniformly sampling the birth of a particle in a cell, MCNP uses the enclosing volume rejection method, which requires the user definition of a volume enveloping the source cell. The randomly sampled points in the volume are accepted as source points only if they fall inside the source cell. Finally, the photon transport estimates $^{*}F8$, which allows the calculation of $H_{\gamma,\mathrm{Tr}}$ (eq. 3).

IV. RESULTS

This section presents and discusses the results of two applications. The first application consists of the delayed heating calculation of an ATR experiment. The second application analyzes the delayed heating in various structures in the RA-6 reactor.

IV.A. ATR experiment

The ATR is a 250-MWth high flux test reactor located at the Reactor Technology Complex of the INL. The ATR was designed to provide an irradiation test environment for conducting a variety of experiments, to study the effects of radiation on reactor structural and fuel materials, and to produce medical and industrial isotopes [42, 43].

The ATR core contains 40 fuel elements arranged in a serpentine annulus between and around nine flux traps, as shown in Figure 3. Each fuel element consists of 19 parallel, curved, aluminum-clad fuel plates forming a 45-degree sector of a right circular cylinder. The fuel arrangement gives the reactor core a clover-leaf configuration, which allows the ATR to be operated at different power levels in the five lobes (NW, NE, C, SW, SE), allowing for independent testing conditions within the same operating cycle. Within each fuel plate, the fuel meat consists of highly enriched (93 wt%) uranium aluminide (UAl_x) fuel powder dispersed in aluminum. Plates 1 through 4 and 16 through 19 contain natural boron carbide (B_4C) powder as a burnable poison.

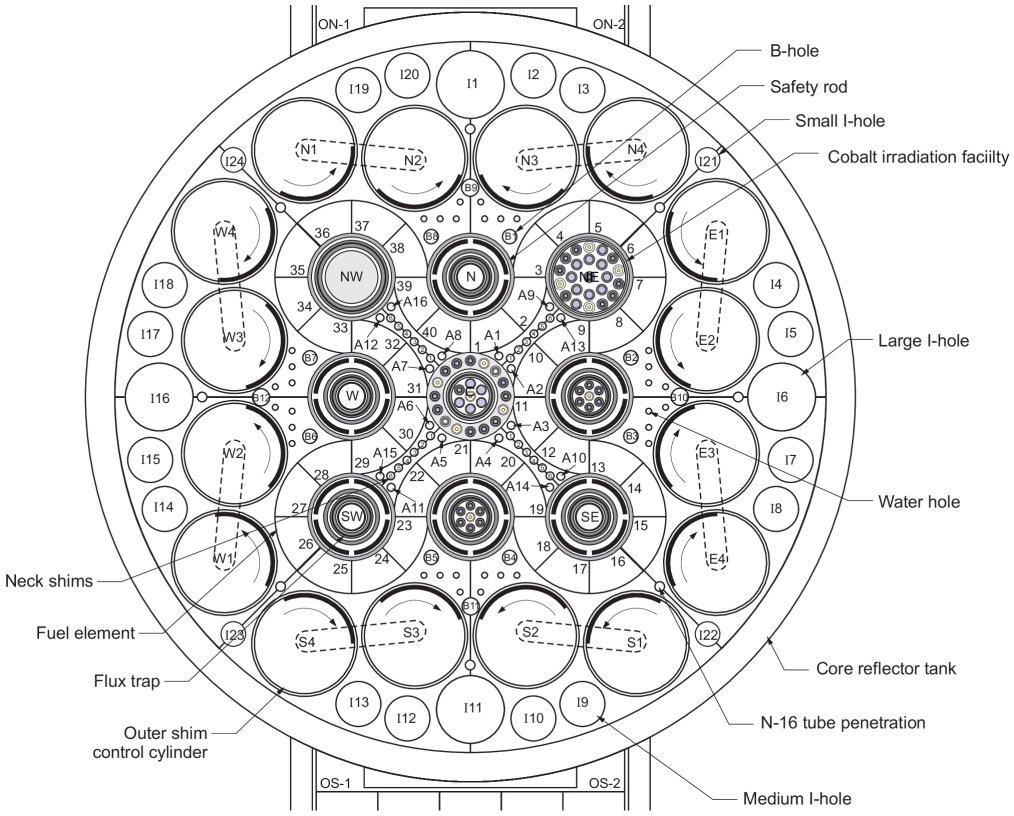

Fig. 3. Top view of the ATR. Image reproduced from [42].

The reactor has 9 flux trap positions and 68 additional irradiation positions inside the reactor core reflector tank. The center capsule facility is surrounded by the H-hole irradiation facility, which contains 10 cobalt baskets, 4 flux monitor holders, and 2 N-16 flow tubes. The neck shim housing is the structural guide for the 24 neck shim and regulating rods, as well as 8 inner and 8 outer A-holes. The beryllium reflector fills the space between the fuel annulus and the core reflector tank, and it hosts the outer shim control cylinders (OSCC), irradiation holes, and water holes. The irradiation holes include a total of 8 small B-holes, 4 large B-holes, 4 small I-holes, 16 medium I-holes, 4 large I-holes, and 4 round and 4 square N-16 monitor holes.

This work uses an MCNP model representing the ATR critical experiment evaluation designated as Cycle 103A-2 that was performed in 1994. This critical evaluation was part of a nuclear re-qualification program that followed the core internals change-out. The critical configuration was defined by the following parameters: 40 fresh fuel elements, OSCC set to 51.8 degrees, 22 shim rods fully inserted, 2 regulating rods fully withdrawn, and 6 safety rods fully withdrawn.

The ATR critical evaluation was first published by the OECD NEA Nuclear Science Committee in the September 2005 Edition of the International Handbook of Evaluated Criticality Safety Benchmark Experiments (ICSBEP Handbook) [42]. The original benchmark model uses the evaluated continuous energy ENDF/B-V cross-section data for 27 °C. This work uses the ENDF/B-VIII.0 cross-section library for the isotopes included in it. The remaining isotopes use the cross-section data of the original model. The model uses 10^4 histories per generation with 250 and 3750 inactive and active cycles. This work considers the reactor composition at the beginning of the equilibrium cycle (BOC) based on the available ATR model.

This demonstration exercise focuses on the delayed heating of the A1 experiment position. The A1 experiment position is an inner A-hole, and it is hosted by the neck shim housing. The diameter of the hole is 0.625 in. This exercise considers an experiment sample made of aluminum.

Although the ATR maximum power rating is 250 MWth, most contemporary experiments do not require such a level, and the reactor operates at a much lower power. This work considers for the calculations a total operating power of 110 MWth that is equally distributed among the five lobes. The irradiation time is 30 days, and the decay is recorded in seven non-uniformly distributed steps up to 12 hours after shutdown.

As the experiment position is in the core region between the fuel assemblies, the calculations

assume that the fission products generate a much higher gamma source intensity than the activation products in the neighboring cells. Hence, the contribution of the reactor components surrounding the experiment is neglected. The only considered contributors to the heating are all the fuel plates and the experiment itself.

IV.B. ATR results

To accommodate the MOAA calculations, the MCNP input file underwent the following modifications. The ATR model defines 19 different material compositions that all fuel elements share for their 19 different fuel plates. The material definitions of each fuel plate were duplicated for each fuel element to allow for their independent definition. Additionally, the volume of each fuel plate was calculated and added into the MCNP input file.

Figure 4 presents the experiment heat production over time. $H_{\gamma,\mathrm{Tr}}$ was calculated for 41 independent photon-transport simulations, wherein each simulation accounts for the contribution to delayed gamma heating of each fuel assembly and the experiment itself.

The gamma heating immediately after shutdown is 849.2 W, and the heating due to charged particles is 56.32 W, which equals to 6.6% of the total heating in the experiment. The self-gamma heating is 5.8 W, which is equal to 0.73% of the total delayed gamma contribution and 0.68% of the total heating. These results show that the self heating in aluminum is very low and validate the initial simplification of neglecting the surrounding structure contributions given that both the experiment and the structures are made of aluminum.

Additionally, the heating due to charged particles decays much faster than the gamma heating and becomes negligible one hour after shutdown. The gamma heating decays to 100 W at approximately six hours after shutdown.

Figure 5 shows the contribution to the total heat in percentage by each fuel assembly and the experiment immediately after shutdown. The largest contributions to the heating in the sample come from the fuel assemblies 1, 10, 40, 2, 11, 9 with contributions of more than 3%. These assemblies are the closest in distance to the experiment position. Additionally, the sample produced a self-heating of 7.3%, from which 6.6% came from the charged particles and 0.7% from the gamma particles.

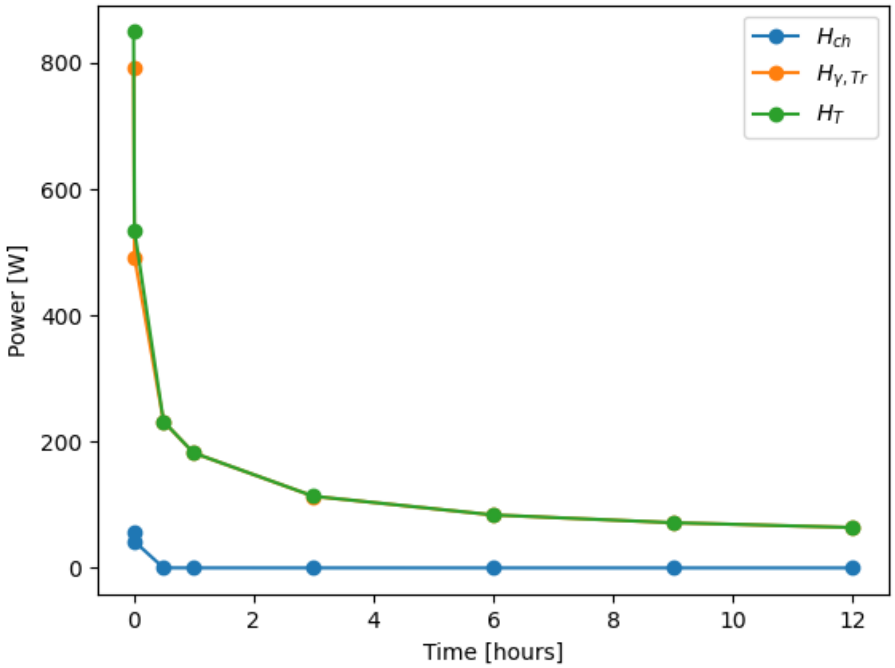

Fig. 4. Shutdown heating rate over time in the ATR A1 experiment position for an aluminum sample.

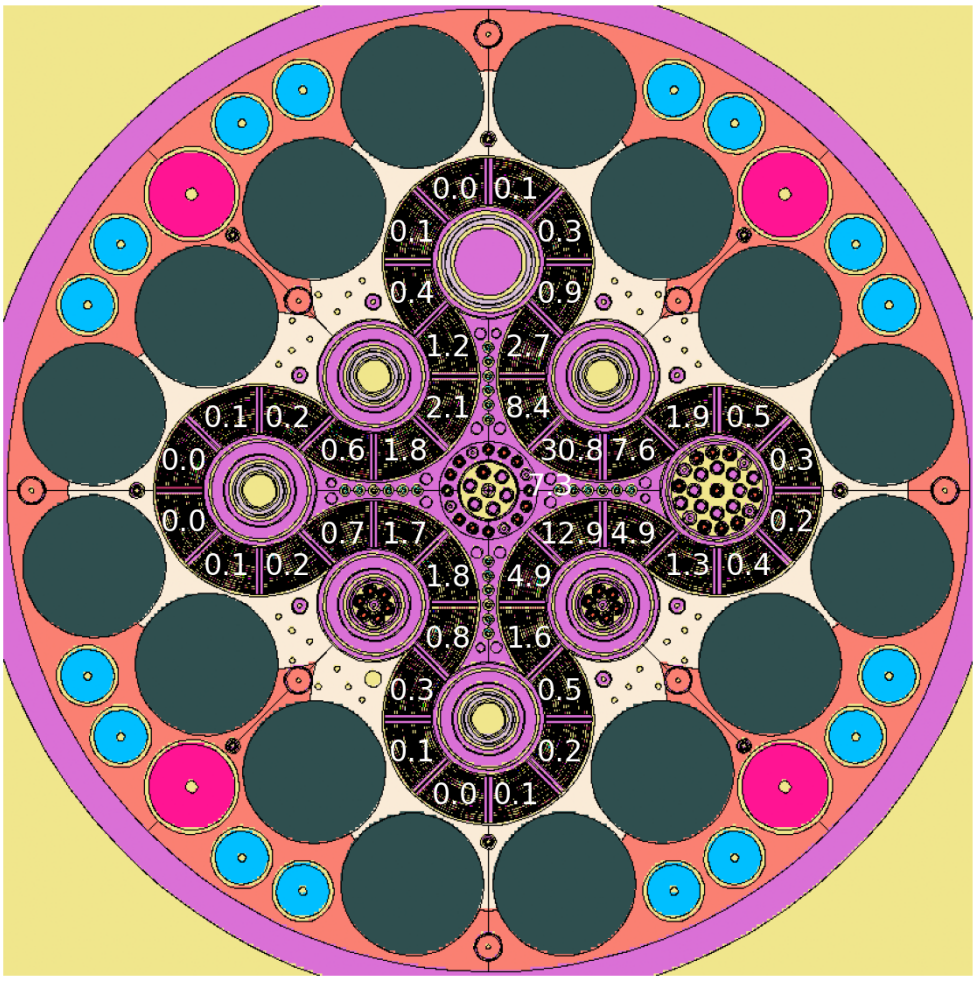

Fig. 5. Contribution by each source to the A1 experiment heat rate immediately after reactor shutdown, with the values expressed in (%). The Figure is based on the MCNP model geometry, which is rotated 45° clockwise with respect to Figure 3.

IV.C. RA-6 structures

The RA-6 is a 3-MWth open pool research reactor located at the Bariloche Atomic Center (CAB), a research and development center of the Argentine National Atomic Energy Commission (CNEA) [42]. It was originally conceived as a teaching tool to support student training at the Balseiro Institute before its uses became diversified. Current applications include neutron activation analysis, neutron radiography, and boron neutron capture therapy (BNCT), among others.

The reactor core is composed of a fuel element arrangement, as shown in Figure 6, that rests on a support grid inside a 2.4-m-diameter, 10.4-m-high stainless steel tank. The tank is filled with demineralized light water, which acts as a coolant, moderator, and reflector. The fuel elements are Material Test Reactor (MTR) type, composed of rectangular fuel plates with aluminum side plates. The fuel meat consists of 19.7% enriched uranium silicide (U_3Si_2) dispersed in an aluminum matrix. There are two types of fuel elements: normal fuel elements (NFEs) and control fuel elements (CFEs). While an NFE is composed of 17 internal and two external fuel plates, a CFE is composed of 14 internal and 4 control guide plates.

The bottom plane of the core assembly rests 8.9-meters-deep on the support grid, which is a 20 cm-thick slab of 99.5% pure aluminum. Primary and secondary cylindrical holes allow the cooling of the internal and external fuel plates, respectively. The primary holes have a diameter of 6.179 cm and are arranged in a rectangular 8 x 10 array with 7.7-cm pitch in the x-direction and 8.1-cm pitch in the y-direction. The secondary holes have a diameter of 2.225 cm and are centered between the primary holes.

On a side of the fuel element arrangement, there is a neutron filter that works as a source for BNCT, as shown in Figure 7. The neutron filter for the BNCT facility is an 87.6-cm-long, 77.1-cm-wide, 82.35-cm-high aluminum container. The filter is filled along the 87.6-cm dimension with the following materials: 17 cm of aluminum bricks, a 0.15-cm-thick cadmium sheet, 10 cm of aluminum, a 0.15-cm-thick cadmium sheet, and the rest is filled with alumina bricks.

The RA-6 reactor operated for 20 years with spent HEU fuel from a higher power reactor and was reconverted to LEU fuel in 2008. The RA-6 critical experiment reported in this evaluation corresponds to the 2008 configuration utilized in the startup program. This critical evaluation was first published by the OECD NEA Nuclear Science Committee in the September 2010 Edition of the ICSBEP Handbook. This work considers the reactor composition at the BOC based on the

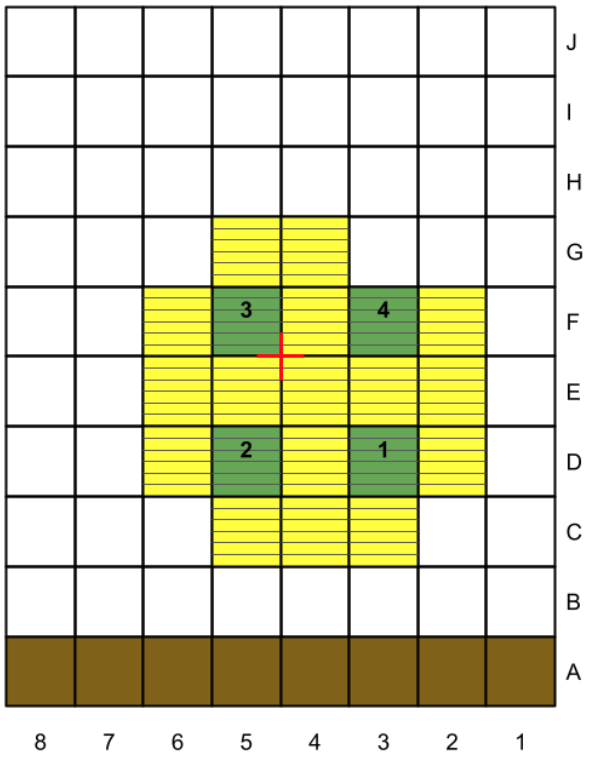

Fig. 6. Top view of the RA-6 critical configuration. NFEs in yellow, CFEs in green, and BNCT filter in brown. Red cross denotes the center of the reactor pool. Image reproduced from [42].

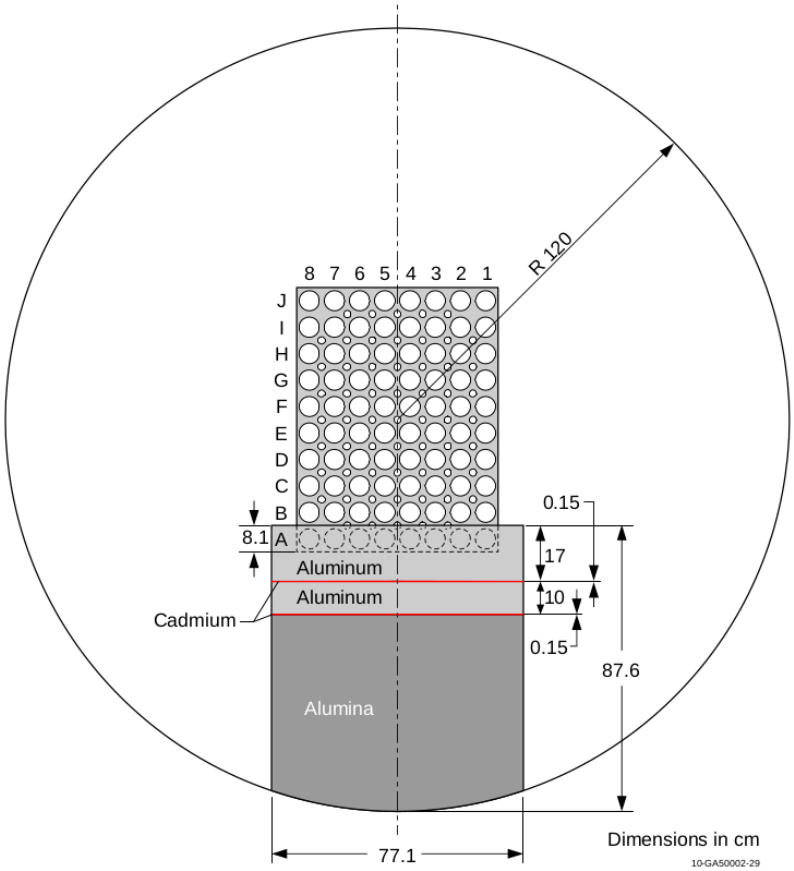

Fig. 7. Top view of the RA-6 support grid and BNCT filter. Image reproduced from [42].

available RA-6 model and uses the evaluated continuous energy ENDF66 cross-section data for 27 °C, which is defined in the original benchmark model. The simulation uses 10^4 histories per generation with 50 and 4000 inactive and active cycles.

Although not shown in the MCNP model, the reactor core has several surrounding components, such as primary pipes, the stainless steel tank, and neutron beam extraction tubes. The analysis of delayed heating in these components could be worthwhile but were omitted as the MCNP model excluded them. Hence, this work calculates the delayed heating on the most important structural components in the model, i.e., the support grid and the BNCT filter.

The RA-6 was originally designed to operate at 1 MWth and the 2008 startup program included a reactor power upgrade to 3 MWth. Although the RA-6 maximum power rating is 3 MWth, it normally operates at a lower power. This work considers operating powers of 1 and 3 MWth and compared their respective results. In this work, the reactor operated for 1 year and the depletion was calculated in four 3-month steps. The considered contributors to the heating are the fuel plates, the support grid, and the BNCT filter.

IV.D. RA-6 results

To accommodate the MOAA calculations, the MCNP input file underwent the following modifications. First, even though the RA-6 model distinguishes between five different types of fuel plates: internal plates in the NFEs, internal plates with burnable poisons in the NFEs, external plates in the NFEs, fuel plate with burnable poisons in the CFEs, and fuel plate without burnable poisons in the CFEs, the original MCNP input file defines all of them with the same material definition. Additionally, several layers of the BNCT filter and the support grid are made of pure aluminum, and the original MCNP input file defines the aluminum only once. Finally, the BNCT filter uses two cadmium layers that share the same material definition in the original MCNP input file. All material definitions of these components were duplicated to allow for their independent definition. Second, the original MCNP input file defines the four CFEs using nested structures with independent cells, but as their definition is identical, a minimal universe renumbering allowed their simultaneous modeling in MOAA. Third, the volume of each fuel plate type, the volume of the different BNCT filter layers, and the volume of the support grid were calculated and added into the MCNP input file.

Figure 8 displays the delayed heating in the support grid and the different BNCT filter layers for operating powers of 1 and 3 MWth, and Table I shows the density of deposited heat in the different structures. The highest deposited heat occurs in the first BNCT layer, while the highest density of deposited heat occurs in the second BNCT layer, which is the first cadmium layer in the filter. For the first, third, and fifth layers of the BNCT filter, the density of deposited heat decreases due to an increase in the spatial distance from the core. However, the fifth layer has a larger deposited heat than the third layer due to its considerably larger volume. The deposited heat in the cadmium sheets is considerably smaller than for the rest of the BNCT layers due to their smaller volume. Table I also shows the comparison between the results for 1 and 3 MWth. A three times fold increase in operation power is translated into an increase in delayed heating of between 2.60 to 2.90 in the reactor structures.

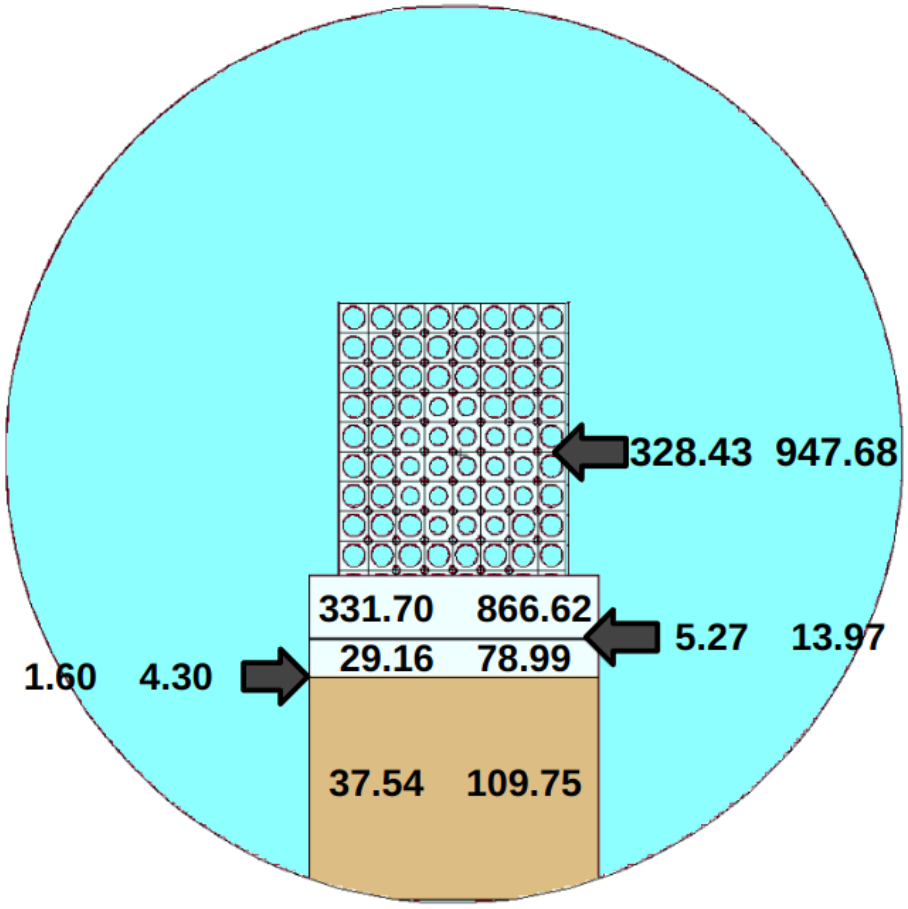

Fig. 8. Delayed heating in the RA-6 reactor structures. Values expressed in W. Left: values corresponding to 1 MWth. Right: values corresponding to 3 MWth.

TABLE I
Main results for delayed heating in the RA-6 reactor structures for an operating power of 1 MWth. V is the cell volume.

	$H_{\mathrm{T,1MW}}/V$ [W · m^{-3}]	$H_{\mathrm{T,3MW}}/V$ [W · m^{-3}]	$\frac{H_{\mathrm{T,3MW}}}{H_{\mathrm{T,1MW}}}$
Support grid	3291.14	9496.55	2.89
BNCT 1st layer	3073.12	8029.02	2.61
BNCT 2nd layer	5533.52	14668.54	2.65
BNCT 3rd layer	459.27	1244.10	2.71
BNCT 4th layer	1680.01	4515.01	2.69
BNCT 5th layer	102.13	298.57	2.92

V. CONCLUSION

Safety analyses in research reactors require the estimation of heat deposited in experiments and reactor structures after reactor shutdown. These analyses establish the heat-source term of those components, and the subsequent thermal-hydraulics calculations determine if an accident could jeopardize their integrity. Additionally, detailed calculations help guide the optimization process of the design of irradiation targets.

In general, existing research reactor safety analyses have a strong focus on the reactor core and assume that the energy released after shutdown is deposited locally in the region of interest. Moreover, many software packages rely on the same assumption, which may be inadequate in some cases. On the other hand, an accurate assessment of the deposited energy across the reactor geometry allows for better determination of the heat removal requirements and ensures an effective cool down. Instead of assuming locally deposited heat, this work utilized detailed methods to target the specific reactor regions.

This article discusses various delayed heating calculation methods, and several publications relying on them. The methods can be summarized into three main approaches: the formal 3-step process, the PIKMT method, and the D1S method. Overall, the discussion gave rise to the choice of an approach for the calculation workflow used in this work. The fact that the formal 3-step process accounts for the activation product decay and the time evolution after shutdown gives the method prevalent attributes over the PIKMT and D1S methods. Therefore, this work introduced a delayed heating calculation workflow based on the formal 3-step process that relies on MOAA.

MOAA is a python package that couples MCNP and ORIGEN to streamline the calculation of the experiment source terms for the ATR and the TREAT. This article briefly discussed the

MOAA workflow, with the main focus on the delayed heating calculation workflow. The delayed heating calculation relies on MOAA for conducting the first two steps of the process, while the third step is conducted by multiple MCNP photon transport simulations.

Finally, this article demonstrated the delayed heating calculation capabilities by presenting two nuclear engineering exercises. These exercises include the delayed heating in an ATR experiment and the RA-6 structures. For the ATR experiment, the results showed the time evolution of the delayed heating up to 12 hours after shutdown as well as the contribution to the heating from the different sources in the reactor. For the RA-6 structures, the results displayed the delayed heating in several of the structural components and the comparison of the heating values for different power levels.

As discussed in the results section, the calculation workflow can accommodate almost any MCNP input file, with some minimal modifications. Overall, this article presented delayed heating capabilities that rely on MOAA and that can be applied to any reactor.

ACKNOWLEDGMENTS

This research made use of the resources of the High Performance Computing Center at the INL, which is supported by the Office of Nuclear Energy of the U.S. Department of Energy and the Nuclear Science User Facilities under Contract No. DE-AC07-05ID14517.

REFERENCES

[1] R. Fairhurst-Agosta and T. Kozlowski, "Decay heat calculations using MCNP and ORIGEN," *presented at American Nuclear Society Student Conference 2022*, Urbana-Champaign, IL (2022).

[2] R. Fairhurst-Agosta and T. Kozlowski, "Machine Learning Classification for Safety Analysis of Nuclear Research Reactor Experiments," *presented at American Nuclear Society Student Conference 2022*, Urbana-Champaign, IL (2022).

[3] R. Fairhurst-Agosta and T. Kozlowski, "Analysis of Nuclear Research Reactor Experiments using Machine Learning," *Transactions of the American Nuclear Society*, **126**, *1*, 352 (2022); doi.org/10.13182/T126-38108.

[4] J. L. Peterson-Droogh and R. H. Howard, "Current Neutronic Calculation Techniques for Modeling the Production of Ir-192 in HFIR," *Proc. Int. Conference on Physics of Reactors 2018 (PHYSOR 2018)*, Cancun, Mexico (2018).

[5] H. Kazeminejad, "Thermal-hydraulic modeling of flow inversion in a research reactor," *Annals of Nuclear Energy*, **35**, *10*, 1813 (2008); doi.org/10.1016/j.anucene.2008.05.006.

[6] A. Hainoun et al., "International benchmark study of advanced thermal hydraulic safety analysis codes against measurements on IEA-R1 research reactor," *Nuclear Engineering and Design*, **280**, 233 (2014); doi.org/10.1016/j.nucengdes.2014.06.041.

[7] A. Abdelmaksoud et al., "Analysis of a Hypothetical Complete Loss-of-Coolant Accident in a Typical Research Reactor," *Nuclear Technology*, **208**, *9*, 1471 (2022); doi.org/10.1080/00295450.2022.2035644.

[8] "Decay Heat Power in Light Water Reactors - an American National Standard," ANSI/ANS-5.1-1994, American Nuclear Society (1994).

[9] J. Leppänen et al., "The Serpent Monte Carlo code: Status, development and applications in 2013," *Annals of Nuclear Energy*, **82**, 142 (2015); doi.org/10.1016/j.anucene.2014.08.024.

[10] L. Giot, "Decay Heat calculations with SERPENT 2," (2018)URL http://montecarlo.vtt.fi/mtg/2018_Espoo/Giot1.pdf.

[11] "SCALE Code System, ORNL/TM-2005/39, Version 6.2.3," ORNL/TM-2005/39, Oak Ridge National Laboratory, Oak Ridge, TN (2018); doi.org/10.2172/1426571.

[12] H. C. Lee et al., "Decay heat analysis of VHTR cores by Monte Carlo core depletion calculation," *Annals of Nuclear Energy*, **37**, *10*, 1356 (2010); doi.org/10.1016/j.anucene.2010.05.011.

[13] G. Ilas et al., "Modeling and Simulations for the High Flux Isotope Reactor Cycle 400," ORNL/TM-2015/36, Oak Ridge National Laboratory, Oak Ridge, TN (2015); doi.org/10.2172/1185903.

[14] G. L. Hawkes, J. W. Sterbentz, and B. T. Pham, "Sensitivity Evaluation of the Daily Thermal Predictions of the AGR-2 Experiment in the Advanced Test Reactor," *Proc. of the ASME 2015 Nuclear Forum*, International Conference on Nuclear Engineering, V001T04A002, San Diego, CA (2015); doi.org/10.1115/NUCLRF2015-49698.

[15] R. Fairhurst-Agosta, A. L. Carter, and J. L. Peterson-Droogh, "Development of the MCNP-ORIGEN Activation Automation tool," 1923–1932 (2022); doi.org/10.13182/PHYSOR22-37565.

[16] R. Fairhurst-Agosta and T. Kozlowski, "Demonstration of Decay Heat Calculations using the MCNP-ORIGEN Activation Automation Tool," *presented at Int. Conference on Engineering Computational Technology*, Montpellier, France (2022).

[17] R. Fairhurst-Agosta and T. Kozlowski, "Database Construction for Nuclear Heating Calculations," *Transactions of the American Nuclear Society*, **127**, *1*, 352 (2022); doi.org/10.13182/T127-39622.

[18] C. J. Werner et al., "MCNP Users Manual - Code Version 6.2," LA-UR-17-29981, Los Alamos National Laboratory, Los Alamos, NM (2017).

[19] M. Lemaire et al., "For a better estimation of gamma heating in nuclear material-testing reactors and associated devices: status and work plan from calculation methods to nuclear data," *Journal of Nuclear Science and Technology*, **52**, *9*, 1093 (2015); doi.org/10.1080/00223131.2015.1009957.

[20] Y. Chen and U. Fischer, "Rigorous MCNP based shutdown dose rate calculations: computational scheme, verification calculations and application to ITER," *Fusion Engineering and Design*, **63-64**, 107 (2002); doi.org/10.1016/S0920-3796(02)00144-8.

[21] R. G. Ambrosek and G. S. Chang, "Improved methodology for temperature predictions in advanced reactors," *presented at 1995 National Heat Transfer Conference*, Portland, OR (1995)URL https://www.osti.gov/biblio/116642.

[22] Y.-K. Lee and K. Sharma, "Tripoli-4 Gamma-Ray Dose Calculation for Spent PWR Fuels," *Proc. Int. Conference on Nuclear Engineering (ICONE)*, **1**, V001T04A014 (2013); doi.org/10.1115/ICONE21-15498.

[23] V. Mozin, "Delayed Gamma-Ray Assay for Nuclear Safeguards," PhD Dissertation, University of California, Berkeley, CA (2011)URL https://escholarship.org/content/qt5mm1v58k/qt5mm1v58k_noSplash_ca99c596dd23532d4de40c098aa706cd.pdf.

[24] M. L. Fensin, J. S. Hendricks, and S. Anghaie, "The Enhancements and Testing for the MCNPX 2.6.0 Depletion Capability," *Nuclear Technology*, **170**, *1*, 68 (2010); doi.org/10.13182/NT10-2.

[25] E. Brun et al., "TRIPOLI-4, CEA, EDF and AREVA reference Monte Carlo code," *Annals of Nuclear Energy*, **82**, 151 (2015); doi.org/10.1016/j.anucene.2014.07.053.

[26] A. Tsilanizara et al., "DARWIN: An Evolution Code System for a Large Range of Applications," *Journal of Nuclear Science and Technology*, **37**, *sup1*, 845 (2000); doi.org/10.1080/00223131.2000.10875009.

[27] T.-Y. Noh, B.-G. Park, and M.-S. Kim, "Estimation of nuclear heating by delayed gamma rays from radioactive structural materials of HANARO," *Nuclear Engineering and Technology*, **50**, *3*, 446 (2018); doi.org/10.1016/j.net.2018.01.010.

[28] R. Forrest and J. Sublet, "FISPACT-99 User manual," UKAEA-FUS-407, United Kingdom Atomic Energy Authority, Culham, United Kingdom (1998)URL http://inis.iaea.org/search/search.aspx?orig_q=RN:31048113.

[29] S. Sheludjakov and A. Serikov, "The advanced 3D method for activation analysis of fusion reactor materials," *Fusion Engineering and Design*, **63-64**, 487 (2002); doi.org/10.1016/S0920-3796(02)00183-7.

[30] P. Sauvan et al., "Development of the R2SUNED Code System for Shutdown Dose Rate Calculations," *IEEE Transactions on Nuclear Science*, **63**, *1*, 375 (2016); doi.org/10.1109/TNS.2015.2507138.

[31] D. Valenza et al., "Proposal of shutdown dose estimation method by Monte Carlo code," *Fusion Engineering and Design*, **55**, *4*, 411 (2001); doi.org/10.1016/S0920-3796(01)00188-0.

[32] L. Petrizzi et al., "Improvement and Benchmarking of the New Shutdown Dose Estimation Method by Monte Carlo Code," *Advanced Monte Carlo for Radiation Physics, Particle Transport Simulation and Applications*, 865–870, Springer, Berlin, Heidelberg (2001); doi.org/10.1007/978-3-642-18211-2_138.

[33] I. Palermo, R. Villari, and A. Ibarra, "Shutdown dose rate assessment with the Advanced D1S method for the European DCLL DEMO," *Fusion Engineering and Design*, **122**, 163 (2017); doi.org/10.1016/j.fusengdes.2017.08.021.

[34] F. B. Brown, W. R. Martin, and R. D. Mosteller, "Monte Carlo - Advances and Challenges," (2008)URL https://mcnp.lanl.gov/pdf_files/TechReport_2008_LANL_LA-UR-08-05891_BrownMostellerEtAl.pdf.

[35] D. Ilas, "Impact of HFIR LEU Conversion on Beryllium Reflector Degradation Factors," ORNL/TM-2013/441, Oak Ridge National Laboratory, Oak Ridge, TN (2013); doi.org/10.2172/1096323.

[36] E. E. Davidson et al., "Heat deposition analysis for the High Flux Isotope Reactor's HEU and LEU core models," *Nuclear Engineering and Design*, **322**, 563 (2017); doi.org/10.1016/j.nucengdes.2017.06.040.

[37] L. Jurbandam, "Calculation of the Fission Q-value and Spatial Energy Deposition in the SAFARI-1 Nuclear Reactor," MS Thesis, University of the Witwatersrand, Johannesburg, South Africa (2018)URL https://wiredspace.wits.ac.za/server/api/core/bitstreams/26b29006-6cae-47c3-bdf0-e53a2ac42bfb/content.

[38] R. Moore et al., "MOCUP: MCNP-ORIGEN2 Coupled Utility Program," INEL-95/0523, Lockheed Martin Idaho Technologies/Idaho National Engineering Laboratory, Idaho Falls, ID (1995); doi.org/10.2172/130667.

[39] H. R. Trellue, "Development of Monteburns: A Code that Links MCNP and ORGEN2 in an Automated Fashion for Burnup Calculations," LA-13514-T, Los Alamos National Laboratory, Los Alamos, NM (1998); doi.org/10.2172/2696.

[40] Z. Xu and P. Hejzlar, "MCODE, Version 2.2: An MCNP-ORIGEN DEpletion Program," MIT-NFC; TR-104, Massachusetts Institute of Technology/Center for Advanced Nuclear Energy Systems, Cambridge, MA (2008)URL http://hdl.handle.net/1721.1/75242.

[41] V. Haeck, "Monte Carlo Depletion Calculation using VESTA 2.1," (2012)URL https://www.oecd-nea.org/science/wpncs/amct/workingarea/meeting2012/20120917_VESTA21_nea.pdf.

[42] Working Party on Nuclear Criticality Safety, "International Criticality Safety Benchmark Evaluation Project," NEA–7231, Organisation for Economic Co-Operation and Development, Nuclear Energy Agency, Issy-les-Moulineaux, France (2014).

[43] T. A. Tomberlin, "Advanced Test Reactor (ATR) Facility 10CFR830 Safety Basis Related to Facility Experiments," *presented at the 12th Annual Energy Facility Contractors Group Safety Analysis Workshop*, Oak Ridge, TN (2002)URL https://inldigitallibrary.inl.gov/sites/sti/sti/3314541.pdf.